DFT models for active sites on high temperature water-gas shift catalysts

R.M. Van Natter, J.S. Coleman, C.R.F. Lund *

Department of Chemical and Biological Engineering, University at Buffalo, 505 Furnas Hall, SUNY, Buffalo, NY 14260-4200, USA

ARTICLE INFO

ABSTRACT

A simple two-step regenerative model for the kinetics of high temperature water-gas shift provided a good fit to published experimental data for a commercial ferrochrome catalyst. The fitting process yielded an enthalpy of localization of oxygen adatoms on the surface equal to $-611\ kJ\ mol^{-1}$, and it predicted that virtually all adsorption sites were covered by oxygen adatoms at reaction conditions. Cluster models were created to represent possible active sites on $\{1\,0\,0\}$, $\{1\,1\,0\}$ and $\{1\,1\,1\}$ surfaces of Fe_3O_4, the active state of the catalyst. Energies of localization of oxygen adatoms on exposed cation sites were calculated using density functional theory. The computed energies were found to vary in proportion to the number of oxygen anions missing from the normal octahedral coordination of the cation adsorption sites. Comparing the results from the kinetic modeling to the computed energies of localization suggests that on average, the active site on the working catalyst is coordinated to 3.2 oxygen anions, not counting the oxygen adatom.

© 2008 Elsevier B.V. All rights reserved.

1. Introduction

Two fundamentally different types of reaction mechanism can be used to model the kinetics of high temperature water-gas shift (HTWGS), reaction (1), over ferrochrome catalysts [1,2]. One type is often referred to as a regenerative or a redox mechanism. Regenerative mechanisms consist of two sub-mechanisms. In one regenerative sub-mechanism, steam oxidizes a site on the catalyst surface, and in the other regenerative sub-mechanism carbon monoxide reduces a previously oxidized site on the catalyst surface. The other type of water-gas shift mechanism is sometimes referred to as an associative mechanism. A distinguishing feature of associative mechanisms is that they cannot be split into two sub-mechanisms that involve alternative oxidation and reduction of the catalyst surface. Associative mechanisms that have been proposed for water-gas shift typically involve species such as formates or bicarbonates as reactive surface intermediates [1,3–9].

$$CO + H_2O \rightleftarrows CO_2 + H_2 \qquad (1)$$

Reaction kinetics alone does not permit discrimination among the different mechanistic kinetic models for HTWGS [10]. Observed kinetics can be equally well described using either regenerative or associative mechanistic models. Similarly, infrared spectroscopy and other techniques provide evidence for the existence of species like formates and bicarbonates [9,11], but they do not provide definitive evidence that such species participate in the primary mechanistic pathways of water-gas shift conversion. Indeed, it can be argued that over ferrochrome catalysts, HTWGS occurs by more than one pathway depending upon the prevailing conditions [2]. The identity of the prevailing mechanism is even less certain for ferrochrome catalysts that are promoted with copper [12].

Computational chemistry might prove useful in discriminating among HTWGS mechanistic possibilities. Before computational chemistry can be used in this way, it is necessary to decide how to best represent the catalytically active site. Real water-gas shift catalysts consist of small particles of Fe_3O_4 (magnetite) to which chromia and other promoters are added. These materials are expected to expose a variety of different surface geometries, each of which might be catalytically active. Either periodic slab type representations or truncated clusters can serve to model the active sites, and each will have specific advantages and disadvantages. In the work reported here, truncated cluster models were employed where each cluster exposed a surface geometry characteristic of one of the low-Miller-index surfaces of magnetite. Small computational clusters are not likely to reproduce the ferrimagnetic properties of magnetite nor the rapid electron hopping among its octahedral cations. As such, it is not clear whether cluster models will be capable of accurately modeling HTWGS active sites. The objective of this work was to explore their suitability in this regard. To do so, a simple two-step microkinetic model has been fit to experimental rate data, yielding an estimate for the heat of localization of a surface oxygen adatom. Density functional theory (DFT) has been used to calculate the heats of localization of a surface oxygen adatom using the cluster models. The resulting values are then compared to assess the adequacy of the cluster models and to find

 * Corresponding author. Tel.: +1 716 645 2911x2211; fax: +1 716 645 3822.
 E-mail address: lund@eng.buffalo.edu (C.R.F. Lund).

Nomenclature

$\Delta H_j^{\ddagger}$	enthalpy of activation for reaction j
ΔH_j°	standard enthalpy of reaction j
$\Delta H_{f,i}^{\circ}$	standard enthalpy of formation of species i at prevailing temperature (calculated from Shomate equation)
$\Delta H_{loc,O}^{\circ}$	enthalpy of localization of an oxygen adatom
k_j	rate coefficient for reaction j
K_j	equilibrium constant for reaction j
m	mass of catalyst in the reactor
$\dot{n}_i$	molar flow rate of species i, a superscript 0 denotes the value at the reactor inlet
P_i	partial pressure of species i; total pressure if no subscript
r_j	rate of reaction j per mass of catalyst
S_i°	standard entropy of species i at prevailing temperature (calculated from Shomate equation)
$\Delta S_j^{\ddagger}$	entropy of activation for reaction j
ΔS_j°	standard entropy of reaction j

Greek letter

θ_i	fractional coverage of surface sites by species i

which exposed surface geometry provides the best representation of the active sites.

2. Experimental

2.1. Microkinetic modeling

The simplest redox-type mechanism that could be written for water-gas shift is given by equations (2) and (3). It is unlikely that reactions (2) and (3) are actually elementary steps, but for present purposes they will be treated as if they are, and the corresponding models will be referred to as microkinetic models instead of mechanistic kinetic models. This microkinetic model is attractive for present purposes because it involves only two surface species: vacant sites (*) and sites containing an oxygen adatom (O–*). Thus for a given cluster model, only two DFT calculations need to be performed, and this facilitates efficient screening of several different cluster models. Furthermore, as will be seen presently, the microkinetic model can be formulated so that it yields a meaningful estimate for the enthalpy of localization of a surface oxygen adatom (provided, of course, that the fit of the microkinetic model to experimental data is sensitive to that parameter).

$$CO + O\text{–}* \rightleftarrows * + CO_2 \qquad (2)$$

$$H_2O + * \rightleftarrows O\text{–}* + H_2 \qquad (3)$$

Bohlbro has conducted an extensive study of the kinetics of HTWGS [13–17], and his data have been used in the microkinetic modeling performed in the present study. The data set includes 189 separate experiments wherein the feed composition, temperature, pressure and mass of catalyst were varied. Bohlbro's experiments were performed in a tubular packed bed reactor that can be modeled as an isothermal, isobaric, steady-state, plug flow reactor. Doing so leads to a reactor model that consists of the coupled set of five differential equations and two algebraic equations given in Table 1. (Bohlbro included nitrogen as a diluent in the feed, hence the additional mole balance equation.)

As noted, reactions (2) and (3) can be treated as if they are elementary, in which case their rate expressions will take the form given in Table 1. Simple transition state theory allows the two rate coefficients appearing in the rate expressions to be written in terms of an entropy of activation, $\Delta S_j^{\ddagger}$, and an enthalpy of activation, $\Delta H_j^{\ddagger}$, for each reaction, j. This is also shown in Table 1. The equilibrium constants appearing in the rate expressions can be written in terms of the entropies, ΔS_j°, and enthalpies, ΔH_j°, of the two reactions, again as shown in Table 1. Finally, the entropies and enthalpies of the two reactions can be expressed in terms of the standard entropies, S_i° and enthalpies of formation, $\Delta H_{f,i}^{\circ}$, of the species, i, participating in the reactions (Table 1).

Combining all the information in Table 1, it can be seen that there are six unknown quantities that appear in the microkinetic model: the entropy of activation for each of reactions (2) and (3), the enthalpies of activation for each of reactions (2) and (3), the entropy of formation of a surface oxygen adatom and the enthalpy of formation of a surface oxygen adatom (the entropy and enthalpy of formation of a vacant site may be taken to equal zero). All other quantities are fundamental constants, experimentally measured quantities, or tabulated thermodynamic quantities (i.e. the thermodynamic data for the gas phase species). Herein, the standard entropies and enthalpies of formation of gas phase CO, CO_2, H_2O, H_2 and N_2 were computed as a function of temperature using the Shomate equation with parameters available from the NIST Chemistry Web Book [18].

In this work, the standard entropy of an oxygen adatom at a given temperature was taken to equal the standard entropy of a gas phase oxygen atom at that temperature (as calculated using Shomate parameters from the NIST Chemistry Web Book) less all three degrees of translational entropy (treating it as an ideal gas at the average experimental temperature and pressure). The standard enthalpy of formation of an oxygen adatom at a given temperature was similarly taken to equal the standard enthalpy of formation of a gas phase oxygen atom at that temperature (similarly calcu-

Table 1
Microkinetic model for water-gas shift

Gas phase mole balances	$\dfrac{d\dot{n}_{CO}}{dm} = -r_2;\quad \dfrac{d\dot{n}_{CO_2}}{dm} = r_2;\quad \dfrac{d\dot{n}_{H_2O}}{dm} = -r_3$ $\dfrac{d\dot{n}_{H_2}}{dm} = r_3;\quad \dfrac{d\dot{n}_{N_2}}{dm} = 0$
Surface mole balance	$r_2 - r_3 = 0$
Conservation of active sites	$\theta_v + \theta_O = 1$
Rate expressions	$r_2 = k_2 P_{CO} \theta_O \left\{ 1 - \dfrac{P_{CO_2} \theta_v}{K_2 P_{CO} \theta_O} \right\}$ $r_3 = k_3 P_{H_2O} \theta_v \left\{ 1 - \dfrac{P_{H_2} \theta_O}{K_3 P_{H_2O} \theta_v} \right\}$
Partial pressures	$P_i = \dfrac{\dot{n}_i}{\dot{n}_{CO} + \dot{n}_{CO_2} + \dot{n}_{H_2O} + \dot{n}_{H_2} + \dot{n}_{N_2}} P$
Rate coefficients	$k_2 = \exp\left[\dfrac{\Delta S_2^{\ddagger}}{R}\right] \exp\left[\dfrac{-\Delta H_2^{\ddagger}}{RT}\right]$ $k_3 = \exp\left[\dfrac{\Delta S_3^{\ddagger}}{R}\right] \exp\left[\dfrac{-\Delta H_3^{\ddagger}}{RT}\right]$
Equilibrium constants	$K_2 = \exp\left[\dfrac{\Delta S_2^{\circ}}{R}\right] \exp\left[\dfrac{-\Delta H_2^{\circ}}{RT}\right]$ $K_3 = \exp\left[\dfrac{\Delta S_3^{\circ}}{R}\right] \exp\left[\dfrac{-\Delta H_3^{\circ}}{RT}\right]$
Entropies and enthalpies of reaction	$\Delta S_2^{\circ} = S_{CO_2}^{\circ} + S_*^{\circ} - S_{CO}^{\circ} - S_{O\text{–}*}^{\circ}$ $\Delta S_3^{\circ} = S_{H_2}^{\circ} + S_{O\text{–}*}^{\circ} - S_{H_2O}^{\circ} - S_*^{\circ}$ $\Delta H_2^{\circ} = \Delta H_{f,CO_2}^{\circ} + \Delta H_{f,*}^{\circ} - \Delta H_{f,CO}^{\circ} - \Delta H_{f,O\text{–}*}^{\circ}$ $\Delta H_3^{\circ} = \Delta H_{f,H_2}^{\circ} + \Delta H_{f,O\text{–}*}^{\circ} - \Delta H_{f,H_2O}^{\circ} - \Delta H_{f,*}^{\circ}$
Initial conditions	$\dot{n}_{CO}(m=0) = \dot{n}_{CO}^{\circ};\ \dot{n}_{CO_2}(m=0) = \dot{n}_{CO_2}^{\circ};$ $\dot{n}_{H_2O}(m=0) = \dot{n}_{H_2O}^{\circ};\ \dot{n}_{H_2}(m=0) = \dot{n}_{H_2}^{\circ};$ $\dot{n}_{N_2}(m=0) = \dot{n}_{N_2}^{\circ}$

lated using the Shomate equation) less an unknown enthalpy of localization at a surface site. This enthalpy of localization, $\Delta H^{\circ}_{\mathrm{loc,O}}$ was treated as a constant and used as an adjustable parameter when fitting the microkinetic model to Bohlbro's experimental data. Thus, by fitting the microkinetic model to Bohlbro's experimental data, using $\Delta S^{\ddagger}_2$, $\Delta S^{\ddagger}_3$, $\Delta H^{\ddagger}_2$, $\Delta H^{\ddagger}_3$ and $\Delta H^{\circ}_{\mathrm{loc,O}}$ as adjustable parameters, it is possible to generate experimental estimates for the values of those parameters.

The mathematical procedures used to solve the reactor design equations and to fit the microkinetic model to the data are analogous to those used and described previously [19]. Briefly, in order to model any one of Bohlbro's experimental data points, the model equations in Table 1 were integrated numerically using the implicit Euler method. The integration step size was chosen to be sufficiently small that it did not affect the result. The initial conditions were simply the inlet molar flow rates of each of the gas phase species for the experiment being modeled, as given in Table 1, and the integration range corresponded to the mass of catalyst used in that experiment. The fitting was also performed numerically by minimizing the sum (over all 189 experimental data points) of the square of the difference between the experimentally measured CO conversion and that predicted by the model. The Nelder–Mead downhill simplex method [20] was employed to find the parameter values that minimized this objective function.

2.2. Cluster models for the active sites

Magnetite is an inverse spinel wherein the oxygen anions adopt a cubic closest packed arrangement, Fe(III) cations are found in tetrahedral sites and equal numbers of Fe(II) and Fe(III) cations are found in octahedral sites. The structure is slightly distorted because the Fe(III) cations are larger than the tetrahedral voids between the oxygen anions. Clusters to represent active sites were created by starting from this crystallographic structure (including the distortion). The structure was first cleaved to generate the desired low-Miller-index surface. A cluster then was formed by cutting additional atoms from what remained. The clusters were always chosen so that they would be symmetric, uncharged, and where possible, so that they would contain an integer number of stoichiometric formula units. This was done because formally, the individual bonds in magnetite involve fractional charges. As such, cut bonds cannot be "healed" in the usual manner by adding a hydrogen atom.

The magnetite structure can be cut perpendicular to each of the [1 0 0], [1 1 0] and [1 1 1] directions so that different surfaces are revealed. Here, in each case, the cut was made so that the surface retained octahedral cations that were not fully coordinated to oxygen anions. This was done because the octahedral cations are the more likely catalytic sites, containing both Fe(II) and Fe(III) cations between which rapid electron hopping occurs. In other words, tetrahedral cations have not been considered as potential active sites in this study. The resulting clusters exposing a {1 1 0} and a {1 1 1} surface each had only a single oxygen adsorption site, but the cluster exposing a {1 0 0} surface had two oxygen adsorption sites. It will be seen later that the microkinetic modeling predicts a very high coverage of the surface by adsorbed oxygen adatoms. Therefore, the clusters were initially created to include an oxygen atom occupying each surface site, and the redox cycle was presumed to involve removal of one adsorbed oxygen atom.

The resulting clusters presenting a {1 0 0}, {1 1 0} or {1 1 1} surface with all oxygen atom adsorption sites occupied are shown in Fig. 1a through 1c, respectively. The cluster representing the {1 0 0} surface, Fig. 1a, contains 35 atoms, that is, five Fe_3O_4 units. Calculations were also performed on a smaller cluster, not shown, that consisted of only two Fe_3O_4 units. The cluster representing the
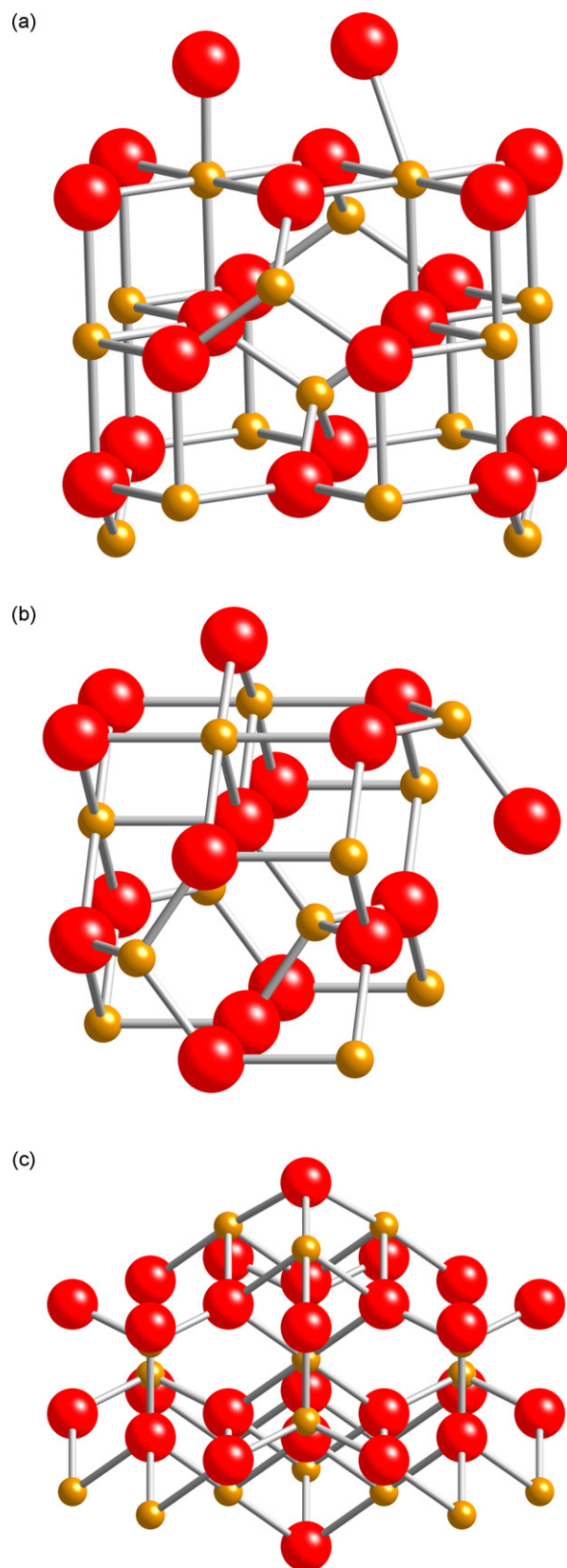

Fig. 1. Clusters used to model the oxygen-covered active site for water-gas shift on magnetite exposing (a) a {1 0 0} surface, (b) a {1 1 0} surface and (c) a {1 1 1} surface. The smaller spheres represent iron cations and the larger spheres represent oxygen anions.

Table 2
Microkinetic model parameters

Parameter	Value
$\Delta H^{\circ}_{\text{loc,O}}$	$-611\,\text{kJ mol}^{-1}$
$\Delta S^{\ddagger}_{2}$	$-142\,\text{J mol}^{-1}\,\text{K}^{-1}$
$\Delta S^{\ddagger}_{3}$	$-145\,\text{J mol}^{-1}\,\text{K}^{-1}$
$\Delta H^{\ddagger}_{2}$	$80.3\,\text{kJ mol}^{-1}$
$\Delta H^{\ddagger}_{3}$	$19.9\,\text{kJ mol}^{-1}$

{1 1 0} surface, Fig. 1b, includes four Fe_3O_4 units. In the case of the cluster representing the {1 1 1} surface, it was not possible to create a cluster that was both symmetric and that contained an integer number of Fe_3O_4 units. Thus, the final, symmetric cluster, Fig. 1c, contains six Fe_3O_4 units plus an additional octahedral Fe atom (charge +2) and an additional O atom (charge −2). Calculations were also performed on a smaller cluster, not shown, that consisted of three Fe_3O_4 units plus one Fe atom and one O atom. The corresponding clusters representing the same surfaces as Fig. 1, but with a single oxygen adatom removed are shown in Fig. 2a through 2c.

2.3. Computational chemistry

The structure and energy of possible catalytic intermediate species were calculated using Jaguar, version 7.0. Density functional theory (DFT) was employed using B3LYP hybrid exchange and correlation functionals and TZV** basis sets. Fine DFT grids were employed, and ultrafine geometry convergence was specified. Symmetry constraints were not imposed upon any of the species investigated. Zero-point energies were not calculated, and corrections were not made for any possible basis set superposition errors. Iron oxides are high spin compounds, and consequently the iron has been assumed to exist in the high spin state.

Jaguar includes a facility for generating starting wavefunctions wherein the formal charge and spin state of each ion can be specified. For the results reported here, it was assumed that the formal charges on the iron ions in a cluster with one oxygen adatom removed from the surface site(s) (that is, the clusters in Fig. 2) correspond to the formal charge state of Fe_3O_4, and that when an oxygen atom is adsorbed (as in Fig. 1), two Fe(II) cations are formally oxidized to Fe(III) cations with the adatom becoming an oxygen anion. The formal spin states used in setting up the initial guesses were consistent with the known ferromagnetic coupling in magnetite. The spatial coordinates of all atoms other than the oxygen adatoms were held fixed at their crystallographic positions as already noted, but when adatoms were present, their location was determined by geometry optimization before any other properties were calculated.

3. Results and discussion

3.1. Two-step microkinetic model

Despite its simplicity, the fit of the two-step microkinetic model to Bohlbro's data set was very good. Fig. 3 presents a parity plot comparing the measured CO conversion to the value predicted by the model for all 189 data. The correlation coefficient for the fit, r^2, was equal to 0.91. The resulting parameter values are presented in Table 2. The magnitudes of the entropies of activation are quite reasonable for reactions involving a gas phase reactant and an activated complex that is localized on the catalyst surface. Specifically, they are close in magnitude to the entropy change that is computed if the gas phase species loses all its translational entropy in forming the activated complex. Similarly, the enthalpies of activation and
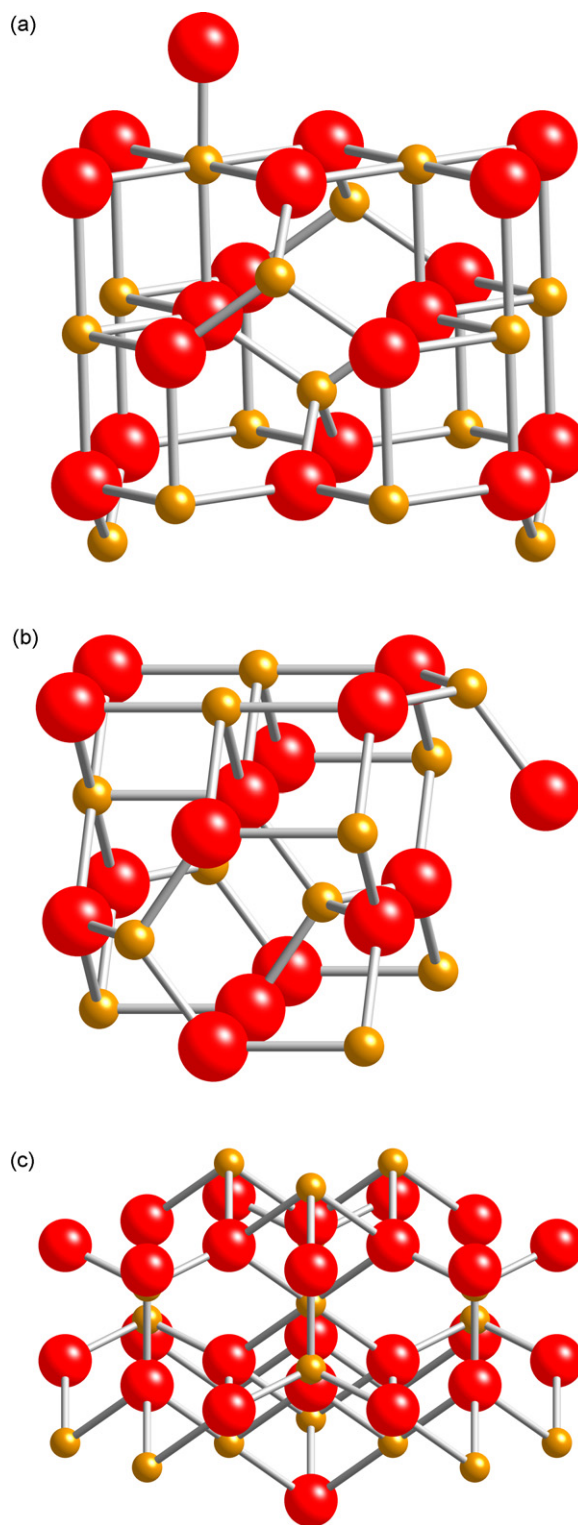

Fig. 2. Clusters used to model the reduced form of the active site for water-gas shift on magnetite exposing (a) a {1 0 0} surface, (b) a {1 1 0} surface and (c) a {1 1 1} surface. The smaller spheres represent iron cations and the larger spheres represent oxygen anions.

the enthalpy of localization of an oxygen atom are of reasonable magnitudes.

When Bohlbro analyzed his data set, he used power-law kinetic models. He used smaller sub-sets of the data to determine apparent reaction orders and activation energy. More importantly, Bohlbro
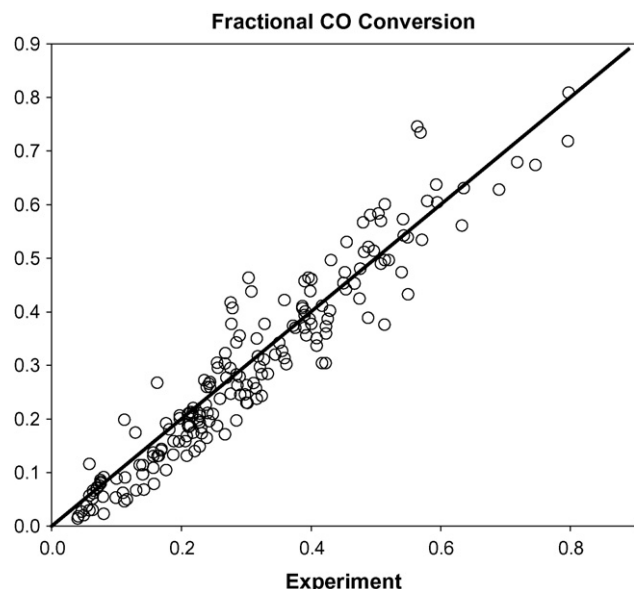
Fig. 3. Parity plot showing the agreement between the measured CO conversion and that predicted by the model.

noted that his catalyst aged under reaction conditions. As a consequence, he performed separate experiments for the purpose of estimating the apparent activation energy of the reaction. The residuals plot presented in Fig. 4 shows the difference between the CO conversion predicted by the present microkinetic model and Bohlbro's measured conversion as a function of temperature. The full data set is plotted, with the experiments Bohlbro used in estimating the activation energy additionally circled. It can be seen that the circled data points do deviate systematically, almost all give negative residuals. However, the magnitudes of the residuals for these selected data points fall within the range of the other data. That is, the size of the selected residuals is not significantly larger than the other data in the set. Hence, the aging that Bohlbro noted is not expected to have caused large errors in the microkinetic model parameters presented in Table 2, but their uncertainties may be somewhat greater than indicated by the correlation coefficient of 0.91.

In generating the microkinetic model, reactions (2) and (3) were treated as if they are elementary steps, but this is not necessarily true. It is quite possible that reactions (2) and (3) are not elemen-
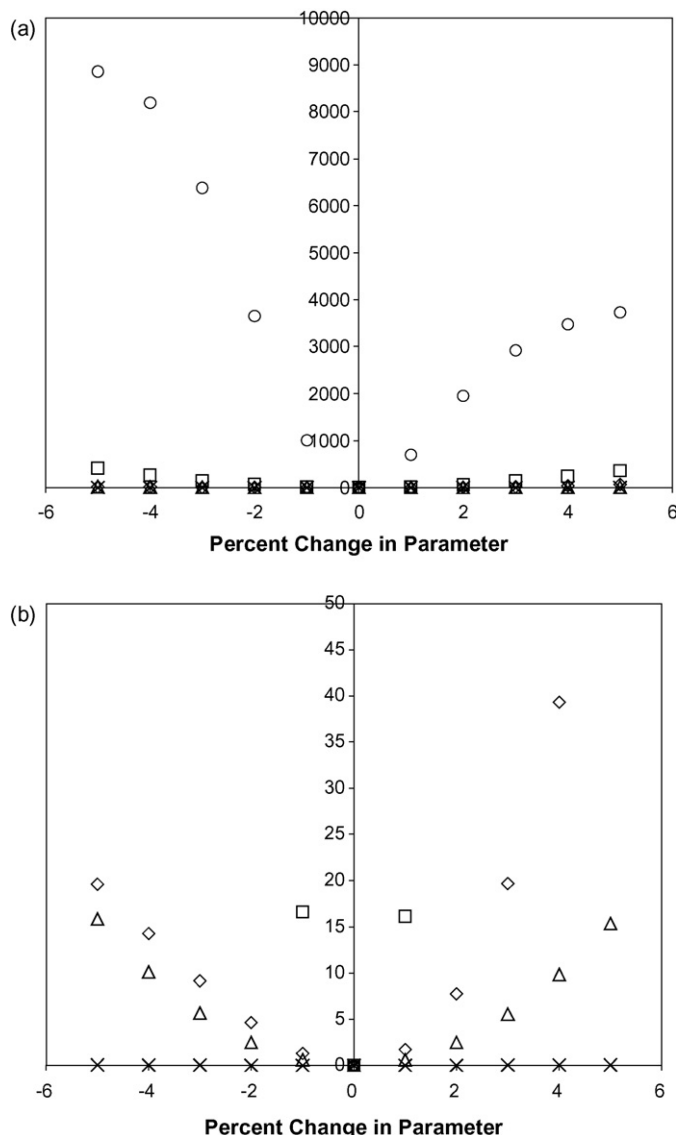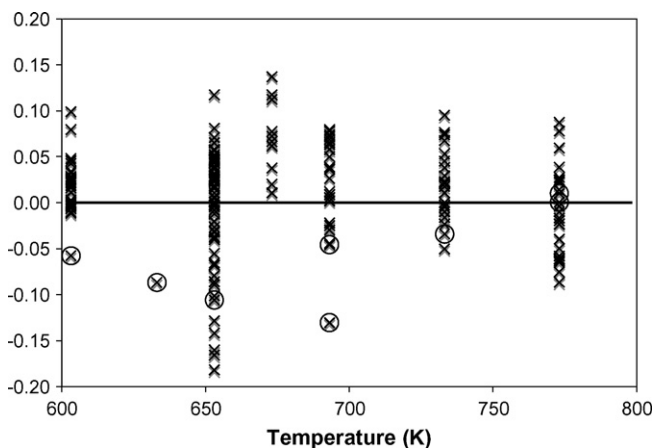

Fig. 4. Residuals (difference between CO conversion from experiment and model) as a function of experimental temperature. The circled data were used by Bohlbro to estimate the activation energy.

Fig. 5. Sensitivity of the sum of the squares of the errors between the model and experiment to variation in each model parameter, holding all other parameters constant at their optimum value. The scale in (a) is much larger than in (b) because the fit is much more sensitive to the value of the enthalpy of localization of oxygen (circles) than to the entropies of activation of reactions (2) and (3) (diamonds and squares, respectively) or to the enthalpies of activations of reactions (2) and (3) (crosses and triangles, respectively).

tary, but instead represent the net effect of two or more molecular events. As a consequence it would not be correct to relate the entropies and enthalpies of activation ($\Delta S_2^{\ddagger}$, $\Delta S_3^{\ddagger}$, $\Delta H_2^{\ddagger}$ and $\Delta H_3^{\ddagger}$) to molecular properties that could be computed using DFT with a transition state search. In contrast, the enthalpy of localization of a surface oxygen adatom, $\Delta H_{loc,O}^{\circ}$, is a thermodynamic quantity associated with an actual surface species. As such, it can be related to molecular properties that can be computed using DFT (given a molecular model for the active site).

Fig. 5 shows that the fit of the microkinetic model to the experimental data is highly sensitive to the value of $\Delta H_{loc,O}^{\circ}$. Specifically the plot shows how the sum of the squares of the residuals changes when each fitting parameter is varied from its optimum value. It is very clear that the fit is much, much more sensitive to the value of $\Delta H_{loc,O}^{\circ}$ than to any other parameter. This means that the value of $\Delta H_{loc,O}^{\circ}$ derived by fitting the model to the data should have

Table 3
Calculated energies of localization of an oxygen adatom

Fe_3O_4 surface	Energy of localization
{1 1 1}	$-668\,kJ\,mol^{-1}$
{1 1 0}	$-378\,kJ\,mol^{-1}$
{1 0 0}	$-112\,kJ\,mol^{-1}$

the least uncertainty among the parameters derived from fitting. Further, it suggests that it should be possible to make meaningful comparisons between this value and one that is computed using DFT. The catalyst aging noted by Bohlbro, makes it difficult to assign an uncertainty to the estimated value of $\Delta H^{\circ}_{loc,O}$. On the basis of additional mechanistic modeling not presented here, the uncertainty in the value of $\Delta H^{\circ}_{loc,O}$ is believed to be of the order of $25\,kJ\,mol^{-1}$.

The microkinetic model was used to predict the fractional surface coverage of oxygen adatoms under reaction conditions. In all cases considered, the model predicted that more than 99% of the sites would have an oxygen atom adsorbed upon them at reaction conditions. This included simulations at the outlet conditions for every experimental data point as well as additional simulations as a function of CO conversion at 700 K.

3.2. Cluster models for the active site

It can be seen that the cluster models do not contain chromium atoms whereas the experimental studies employed commercial ferrochrome catalysts. It is well established [2,21–25] that chromia is a textural promoter which serves to stabilize the active surface area of catalysts in which it is used. In particular, the addition of chromia does not change the specific rate of reaction, the reaction orders or the apparent activation energy. The presence of the chromium cations in the iron oxide lattice is believed to lower the rate of diffusion of iron cations and thereby to reduce the rate of sintering of the catalyst [2]. As such, the absence of chromium atoms in the cluster models is not expected to affect the present results.

DFT was used to compute the self-consistent field (SCF) energy for each cluster considered (after geometry optimization, where appropriate), and also for a gas phase oxygen atom. The results were used to calculate the energy of localization corresponding to formation of an oxygen adatom on each of the cluster surfaces. The results for the cluster models shown in Figs. 1 and 2 are presented in Table 3. As already noted, these small cluster models are expected to have deficiencies with respect to predicting bulk magnetic properties and electron hopping phenomena. It is not known whether these inaccuracies will also include calculated surface binding energies. Normally an uncertainty in the energy of localization of the order of $14-17\,kJ\,mol^{-1}$ might be expected, but in the present case the uncertainty may be greater.

The size of the cluster had a substantial effect upon the calculated energy of localization of an O adatom. Initially a 3 formula unit cluster exposing a {1 1 1} surface and a 2 formula unit cluster exposing a {1 0 0} surface were examined. The energy of localization of an O adatom on a {1 1 1} surface was $-934\,kJ\,mol^{-1}$ when the 3 formula unit cluster was used compared to $-668\,kJ\,mol^{-1}$ when the 6 formula unit cluster was used. Similarly, for the {1 0 0} surface, the energy of localization of an O adatom calculated using a 2 formula unit cluster was $-174\,kJ\,mol^{-1}$ compared to $-112\,kJ\,mol^{-1}$ when using a 5 formula unit cluster. It was not computationally practical to use clusters larger than those reported in Table 3, even though these results suggest that the energies of localization of an O adatom presented there may not be converged with respect to the effect of cluster size. At the least, they reinforce the earlier state-

ment that uncertainty in the energies of localization are greater than would normally be expected.

As noted previously, the microkinetic model predicts that effectively every site on the working catalyst has an oxygen adatom adsorbed upon it. This raises the question of what formal charges to assign to the iron cations in the cluster models. One possibility would be to take the oxygen covered cluster models (Fig. 1) to correspond to formal charges for Fe_3O_4. For the {1 0 0} cluster, as an example, this gives five tetrahedral Fe^{3+} cations, five octahedral Fe^{3+} cations and five octahedral Fe^{2+} cations. Then, when the adsorbed oxygen adatom was removed (Fig. 2), there would be five tetrahedral Fe^{3+} cations, three octahedral Fe^{3+} cations and seven octahedral Fe^{2+} cations. In this case, the *most* oxidized species in the redox cycle of Eqs. (2) and (3) would correspond to Fe_3O_4. The alternative possibility would be to assume that Fe_3O_4 is the *least* oxidized species in the redox cycle. In that case, the cluster in Fig. 1a (oxygen covered {1 0 0} surface) would contain five tetrahedral Fe^{3+} cations, seven octahedral Fe^{3+} cations and three octahedral Fe^{2+} cations while the cluster in Fig. 2a (one oxygen removed from the {1 0 0} surface) would contain five tetrahedral Fe^{3+} cations, five octahedral Fe^{3+} cations and five octahedral Fe^{2+} cations. Calculations were performed for both of these possibilities. For the cluster exposing the {1 1 1} surface the first alternative (Fe_3O_4 corresponding to the most oxidized state) the energy of oxygen localization was found to equal $-679\,kJ\,mol^{-1}$, and for the second alternative (Fe_3O_4 being the least oxidized state) the energy of oxygen localization was found to equal $-668\,kJ\,mol^{-1}$. The difference is quite small, and the latter alternative was used in generating the results in Table 3.

Table 3 shows that the energy of oxygen localization becomes more negative upon moving from the {1 0 0} to the {1 1 0} to the {1 1 1} surfaces. This is not surprising. The exposed octahedral cation on the vacant {1 0 0} surface, Fig. 2a, is already coordinated to five other anions. The exposed octahedral cation on the vacant {1 1 0} surface, Fig. 2b, is coordinated to four anions while that on the {1 1 1} surface is coordinated to only three anions. Indeed, analysis of these data shows that the computed energy of localization of an oxygen adatom onto an octahedral cation site is directly proportional to the number of other anions coordinated to that cation. As the existing coordination of the vacant octahedral site cation increases, the energy of localization of an additional oxygen adatom becomes more positive.

3.3. Comparison of experimental and computational results

Fitting the microkinetic model to experimental data gave a value of $-611\,kJ\,mol^{-1}$ for the enthalpy of localization of oxygen on the ferrochrome surface. The closest computed value is $-668\,kJ\,mol^{-1}$ for the energy of localization of oxygen on the cluster model exposing a {1 1 1} surface. The difference, $57\,kJ\,mol^{-1}$ is significant, even after accounting for the uncertainties in the values. There are many possible reasons for the poor agreement, and a few can be offered here. First, it is likely that the real catalyst exposes a variety of different surfaces. As such, the value obtained from the fit represents some sort of weighted average of the values for the surfaces actually exposed by the real commercial catalyst. If this interpretation is accepted, the proportionality with the energy of localization suggests that on average each vacant octahedral cation site is coordinated to 3.2 oxygen anions. An alternative possibility, already discussed, is that the computational clusters are still too small, and that increasing the size of the clusters would eventually lead to a situation where the computed localization energy of one of the clusters would equal the experimental value to within their uncertainties. A third possibility is that the regenerative microkinetic

model is not an accurate representation of the mechanistic pathway, but this seems unlikely since the model fits the data so well and other independent measurements are consistent with it [26,27].

As just discussed, the results suggest that the catalyst surface most nearly resembles a {1 1 1} surface. The experimental oxygen adatom localization enthalpy falls between the energy computed for the {1 1 1} and {1 1 0} surfaces, but closer to the former. It has been mentioned that this might suggest that the real catalyst predominantly exposes features characteristic of these two surfaces. This is not unreasonable in that natural octahedral crystals of Fe_3O_4 typically expose {1 1 1} surfaces, and less common natural dodecahedral crystals expose {1 1 0} surfaces [28]. Atomistic calculations suggest that the {1 1 1} surface of Fe_3O_4 is thermodynamically stable [29]. This surface has been imaged many times using scanning tunneling microscopy and has been found to be stable following high temperature annealing and during thermal desorption of water [30,31]. Thus, it is reasonable that the majority of the active sites for water-gas shift on Fe_3O_4 catalysts should resemble sites found on the {1 1 1} surface.

4. Conclusions

A simple two-step microkinetic model based upon reactions (2) and (3) provides a very good description of the kinetics of high temperature water-gas shift over a commercial ferrochrome catalyst. The model can be formulated so that the enthalpy of localization of an oxygen adatom appears as one of the unknown model parameters. The fit of the microkinetic model to the experimental data is most sensitive to this particular parameter, and consequently a good estimate for its value can be obtained. Using Bohlbro's published data set to do so resulted in a value of -611 kJ mol^{-1} for the enthalpy of localization of a surface oxygen adatom.

Density functional theory was used to calculate corresponding energies of oxygen adatom localization on octahedral cation sites typical of the {1 0 0}, {1 1 0} and {1 1 1} surfaces of Fe_3O_4. These calculations used cluster models to represent the catalyst sites, and while clusters containing as many as 6 formula units of Fe_3O_4 were used, it is possible that the cluster size influenced the results. Nonetheless, the computed energies of localization were found to vary linearly in proportion to the number of oxygen anions missing from the normal octahedral coordination of the cation adsorption sites. The experimental enthalpy of localization was between the energies computed for the {1 1 1} and {1 1 0} surfaces, but much

closer to that of the {1 1 1} surface. This suggests that the active sites on the real catalyst are similar to those found on the {1 1 1} surfaces of magnetite.

References

[1] C.R.F. Lund, J.E. Kubsh, J.A. Dumesic, The role of solid state chemistry in catalysis, in: ACS Symposium Series, vol. 279, 1985, p. 313.
[2] C. Rhodes, G.J. Hutchings, A.M. Ward, Catal. Today 23 (1995) 43–58.
[3] Y. Kaneko, S. Oki, J. Res. Inst. Catalysis, Hokkaido Univ. 13 (1965) 55.
[4] Y. Kaneko, S. Oki, J. Res. Inst. Catal., Hokkaido Univ. 13 (1965) 169.
[5] Y. Kaneko, S. Oki, J. Res. Inst. Catal., Hokkaido Univ. 15 (1967) 185.
[6] R. Mezaki, S. Oki, J. Catal. 30 (1973) 488–489.
[7] S. Oki, R. Mezaki, J. Phys. Chem. 77 (1973) 447–452.
[8] S. Oki, R. Mezaki, J. Phys. Chem. 77 (1973) 1601–1605.
[9] C. Diagne, P.J. Vos, A. Kiennemann, M.J. Perrez, M.F. Portela, React. Kinet. Catal. Lett. 42 (1990) 25–31.
[10] V. Glavacek, M. Marek, M. Korzhinkova, Kinet. Katal. 9 (1968) 1107–1110.
[11] N.A. Rubene, A.A. Davydov, A.V. Kravtsov, N.V. Usheva, S.I. Smol'yaninov, Kinet. Katal. 17 (1976) 465–471.
[12] C. Rhodes, G.J. Hutchings, Phys. Chem. Chem. Phys. 5 (2003) 2719–2723.
[13] H. Bohlbro, Act. Chem. Scand. 15 (1961) 502–520.
[14] H. Bohlbro, Acta Chem. Scand. 16 (1962) 431–438.
[15] H. Bohlbro, Acta Chem. Scand. 17 (1963) 1001–1011.
[16] H. Bohlbro, J. Catal. 3 (1964) 207–215.
[17] Bohlbro, H., An investigation on the conversion of carbon monoxide with water vapour over iron oxide based catalysts, Haldor Topsøe, Gjellerup, Copenhagen, 1969.
[18] NIST Chemistry WebBook, NIST Standard Reference Database Number 69, National Institute of Standards and Technology, Gaithersburg, MD, 20899 (http://webbook.nist.gov), 2005.
[19] C. Sang, B.H. Kim, C.R.F. Lund, J. Phys. Chem. A 109 (2005) 2295–2301.
[20] J.A. Nelder, R. Mead, J. Comput. 7 (1965) 308–313.
[21] A.M. Alekseev, I.P. Kirillov, V.V. Kostrov, Izvestiya Vysyshikh Uchebnykh Zavedenii Khimiya i Khimicheskaya Tekhnologiya 10 (1967) 308–313.
[22] F. Domka, A. Basinska, R. Fiedorow, Surf. Technol. 18 (1983) 275–282.
[23] F. Domka, A. Basinska, W. Przystajko, R. Fiedorow, Surf. Technol. 21 (1984) 101–108.
[24] M.A. Edwards, D.M. Whittle, C. Rhodes, A.M. Ward, D. Rohan, M.D. Shannon, G.J. Hutchings, C.J. Kiely, Phys. Chem. Chem. Phys. 4 (2002) 3902–3908.
[25] M.I. Markina, G.K. Boreskov, F.P. Ivanovskii, B.G. Lyudkovskaya, Kinetika i Kataliz 2 (1961) 867–871.
[26] J.E. Kubsh, J.A. Dumesic, AIChE J. 28 (1982) 793–800.
[27] M. Tinkle, J.A. Dumesic, J. Catal. 103 (1987) 65–78.
[28] C. Klein, Manual of Mineralogy, 21 ed., Wiley, New York, 1993.
[29] M.W. Finnis, Phys. State Sol. A 166 (1998) 397–416.
[30] Y. Joseph, C. Kuhrs, W. Ranke, M. Ritter, W. Weiss, Chem. Phys. Lett. 314 (1999) 195–202.
[31] A.R. Lennie, N.G. Condon, F.M. Leibsle, P.W. Murray, G. Thornton, D.J. Vaughn, Phys. Rev. B 53 (1996) 10244–10253.